

## Scan Range Analysis According to Variation of Einzel Lens Electrode Gap in Microcolumn†

OM KRISHNA SUWAL<sup>1</sup>, ANJLI SHARMA<sup>2</sup>, DAE-WOOK KIM<sup>1</sup>, TAE-SIK OH<sup>1</sup>, HO-SEOB KIM<sup>1</sup>, YOUNG JUNG KIM<sup>2</sup> and YOUNG-CHUL KIM<sup>3,\*</sup>

<sup>1</sup>Department of Physics and Nanoscience, College of Engineering, Sun Moon University, Asan-si, Chungnam 336-708, Republic of Korea

<sup>2</sup>Department of Advanced Materials Engineering, College of Engineering, Sun Moon University, Asan-si, Chungnam 336-708, Republic of Korea

<sup>3</sup>Department of Optometry, Eulji University, 212 Yangji-dong, Sujeong-gu, Seongnam-si, Gyeonggi-do 461-713, Republic of Korea

\*Corresponding author: E-mail: yckim@eulji.ac.kr

Published online: 1 March 2014;

AJC-14785

Microcolumn is a miniaturized electron optical system having a miniaturized electron emitter, electrostatic source lenses, deflectors and an Einzel lens. The optimization of each components are still technically challenging for aberration-free e-beam operation, high quality imaging and large field of view. This paper discusses the influence of gap between Einzel lens electrodes on scan range and focusing nature in various modes of operation. In source lens focusing mode, the scan range is found to be increased with reducing the gap, but the result was opposite in two lens focusing mode where both source and Einzel lens were used for focusing the beam. We also proved these results through simulation analysis on electron beam trajectory and electric field.

**Keywords:** Microcolumn, Scan range, Microfabrication, Electrostatic lens, MEMS.

### INTRODUCTION

A microcolumn is a miniaturized low voltage electron beam (e-beam) device for e-beam lithography<sup>1</sup>, low voltage miniaturized scanning electron microscopy (LV-SEM)<sup>2</sup>, electron beam testing<sup>3</sup> and inspection<sup>4</sup>. The column is composed of electrostatics components and optimized for low voltage operation. Several papers<sup>5-9</sup> reported improved electron beam microcolumns which have the resolution of 10 nm with 1 nA beam current at 1 mm working distance. The schematic diagram of a microcolumn is presented in Fig. 1. The major components of microcolumn are an electron emitter as an e-beam source, a source lens for extracting, accelerating and limiting electron beam, deflectors or scanner for defining deflection range and magnification and an Einzel lens for focusing e-beam without altering its energy. These components are mostly made of Si and they are basically fabricated following the micro-electro-mechanical system (MEMS) technology. The technique allows us to miniaturize the components down to micrometer size and the final dimension of a microcolumn will be 10 or 20 mm in its height and lateral diameter. The small size allows the columns to be assembled into arrays and operated in parallel, providing high-throughput in imaging or lithography<sup>7,10</sup>.

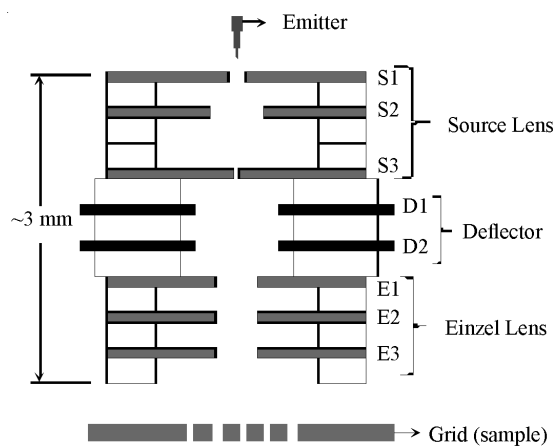


Fig. 1. A schematic representation of a microcolumn

The performance of a microcolumn is predominantly affected by electron optical lenses. For example, chromatic aberration decreases linearly with spacing between electrodes for a fixed working distance<sup>11</sup> and the image quality is affected by perfectness of electrostatic lens which includes circularity and edge smoothness of aperture, accurate alignment of multiple apertures and optimization of electrode thickness and gap between electrodes<sup>12</sup>. However, there are still several technical challenges

†Presented at The 7th International Conference on Multi-functional Materials and Applications, held on 22-24 November 2013, Anhui University of Science & Technology, Anhui, P.R. China

in achieving larger field of view with better resolution. We investigated the influence of spatial gap between Einzel lens electrodes on the field of view and image quality. In this work, a MEMS fabrication technique for making thin Si membrane lenses will be presented and then the results of evaluations on the microcolumn performance such as the scan range and image quality will be discussed with the aid of simulation analysis.

## EXPERIMENTAL

**Methods and methodology:** A single crystalline Si substrate was used for making a thin Si membrane electrostatic lens with a geometrically well-defined circular aperture. Thin electrostatic lenses were fabricated following a sequence of MEMS processes such as photo-lithography, anisotropic etching, deep reactive ion etching (DRIE) and wet etching of bulk Si. The fabrication process is presented in Fig. 2.

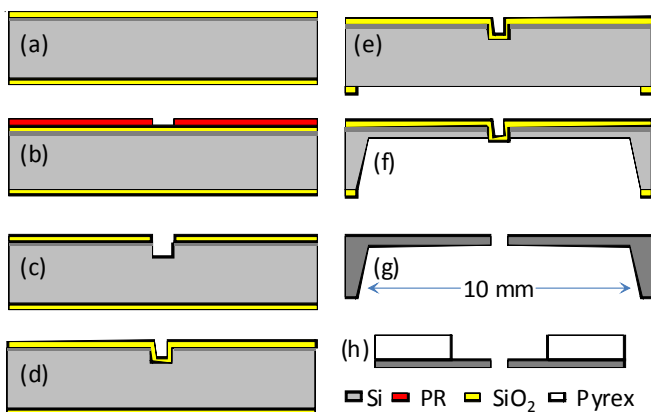


Fig. 2. Fabrication process for an electrostatic lens. (a) Boron doping and oxidation, (b) Photolithography, (c) DRIE for Si trenches, (d) Re-oxidation, (e) Back side patterning, (f) Back side Si etching, (g) Oxide strip off and (h) Pyrex bonding and membrane detachment

A barrier layer was prepared on the front surface of Si wafer by silicon nitride deposition or oxidation process (Fig. 2a), followed by photolithography to transfer circular patterns on photoresist coated Si wafer (Fig. 2b). Silicon oxide or silicon nitride pattern was etched out in a reactive ion etching (RIE) chamber and the wafer was transferred to a deep reactive ion etcher (DRIE) for 10  $\mu\text{m}$  Si trenches (Fig. 2c). After forming the deep trench, silicon oxide layer was grown on Si trenches (Fig. 2d) to protect them during backside Si etching process. Photo-lithography process for backside Si etching was performed and followed by backside etch window opening using RIE (Fig. 2e). After several hours wet Si etching, Si membrane was released with circular silicon oxide membrane at Si trenches (Fig. 2f). Stripping off the silicon oxide, a Si membrane lens with a circular aperture (Fig. 2g) was obtained. In order to increase the conductivity of the electrostatic lens, boron was heavily doped on the Si membrane. After then, electrostatic lenses are anodically bonded to pre-fabricated Pyrex chip (Fig. 2h). Fig. 3(a-c) present SEM images acquired after DRIE, wet Si etching and oxide strip-off, respectively.

The fabricated three lenses were precisely aligned along the optical axis using laser diffraction technique in order to complete a source or Einzel lens set. The alignment was checked

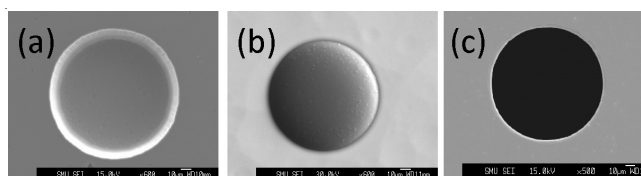


Fig. 3. SEM images acquired after some major fabrication steps. (a) Top view of circular Si trench, *i.e.*, after the process of Fig. 2c, (b) circular oxide membrane released after back side Si etching, *i.e.*, after the process of Fig. 2f, (c) circular Si aperture after oxide strip-off, *i.e.*, after the process of Fig. 2g

checked by the transmission optical microscope images obtained at each lens plane by changing the focal plane from bottom lens to top lens.

To study the effect of Einzel lens structures, two sets of Einzel lenses with different gaps between the electrodes were prepared. The gaps were 150 and 500  $\mu\text{m}$ . These two types of Einzel lenses were assembled into two types of microcolumns named as type-N and type-W, respectively. We obtained sample current images of a Cu grid using both type of microcolumns. The microcolumns were operated in two different modes: (i) one lens focusing mode in which either S2 (S2 focusing mode) or E2 (E2 focusing mode) electrode is biased for focusing electron beam and (ii) two lens focusing mode in which both S2 and E2 electrodes are biased simultaneously.

We analyzed the scan ranges using sample current images obtained in both operation modes for both types of microcolumns. Also, simulation analysis on the electric potential and field by 2D modeling together with electron beam trajectory variations depending on microcolumn operation modes by 3D modeling have been carried out using commercial simulation tools.

## RESULTS AND DISCUSSION

Fig. 4(a) and (b) show the electron micrographs of a Cu grid obtained with type-N and type-W microcolumns at the working distance of 5 and 7 mm, respectively, in S2 focusing operation mode. Tip voltage was -300 V and deflector voltage was  $\pm 100$  V in both cases. The images show that more meshes are observed in the micrograph obtained with type-N than that with type-W, which indicates that the scan range of type-N microcolumn is larger than that of type-W.

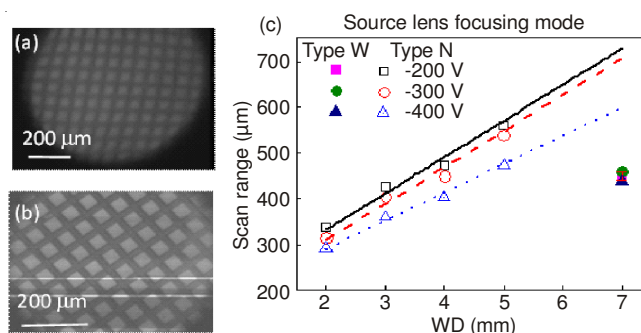


Fig. 4. SEM images of a Cu grid sample acquired with (a) type-N and (b) type-W microcolumn. The mesh size of the Cu grid is 400/inch. (c) Experimental plot of scan range versus working distance obtained at tip voltages of -200, -300 and -400 V for both microcolumns

We repeated the experiments by varying the tip voltages and the working distances for both microcolumns in S2 focusing operation mode. Fig. 4(c) presents a plot for scan range versus working distance for tip voltages of -200, -300 and -400 V. The open symbols represent the scan ranges for type-N microcolumn and solid symbol for type-W. The scan range is observed to be larger for lower electron beam energy and the linear fitting lines depict that scan range increases monotonously with WD for type-N microcolumn. In case of type-W microcolumn, the scan range is observed to be unaltered with the variation of tip voltage and it is smaller than that of type-N microcolumn whereas the WD for type-W is larger (7 mm) than that of type-N microcolumn (2-5 mm). This clearly indicates that the scan range is larger for type-N microcolumn than that for type-W microcolumn.

To see the effects of gap in another operation mode, both columns are operated in E2 focusing mode where the focusing voltage is applied to E2 electrode only and other electrodes are grounded. We were able to capture clear and resolved images from type-W microcolumn, but unable to get clear images from type-N.

Fig. 5(a-d) are the electron micrographs acquired from type-W microcolumn at the tip voltages of -350, -400, -450 and -500 V, respectively. The images seem to be clear and get magnified with the increase of tip voltage. The variation of scan range with tip voltage is plotted in Fig. 5(e). The plot depicts that the scan range increases linearly with reduced negative tip voltages which shows linear dependency and the increment is measured to be  $0.704 \pm 0.036 \mu\text{m}/\text{V}$ .

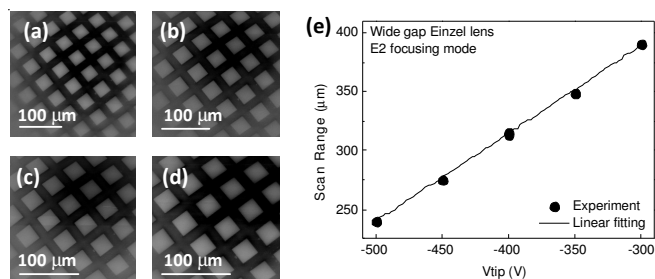


Fig. 5. Electron micrographs of a grid sample and plot for scan range versus tip voltage from type-W microcolumn measured in E2 focusing mode. Images (a-d) were acquired at tip voltages of -350, -400, -450 and -500 V, respectively. The mesh size of the Cu grid was 400/inch. The graph (e) represents a plot for scan range versus tip voltage with the corresponding linear fitting line

On the contrary, the images obtained with type-N microcolumn in E2 focusing mode look unclear and severely distorted as typically shown in Fig. 6(a) which was obtained with the E2 focusing voltage of +410 V with other electrodes grounded. It seems that the electron beam is not properly focused on the sample and the beam path is disturbed. In order to understand the reason for this undesired result, the distribution of electric potential and field strength inside the Einzel lens system have been investigated through computer simulation with 2D modeling by varying the gap between electrodes of Einzel lens.

The electric potential distributions in the Einzel lens region for type-N and type-W microcolumns are presented in Fig. 6(b) and (c). For this simulation, a focusing voltage of 100 V was applied to the central electrode (E2) and other electrodes

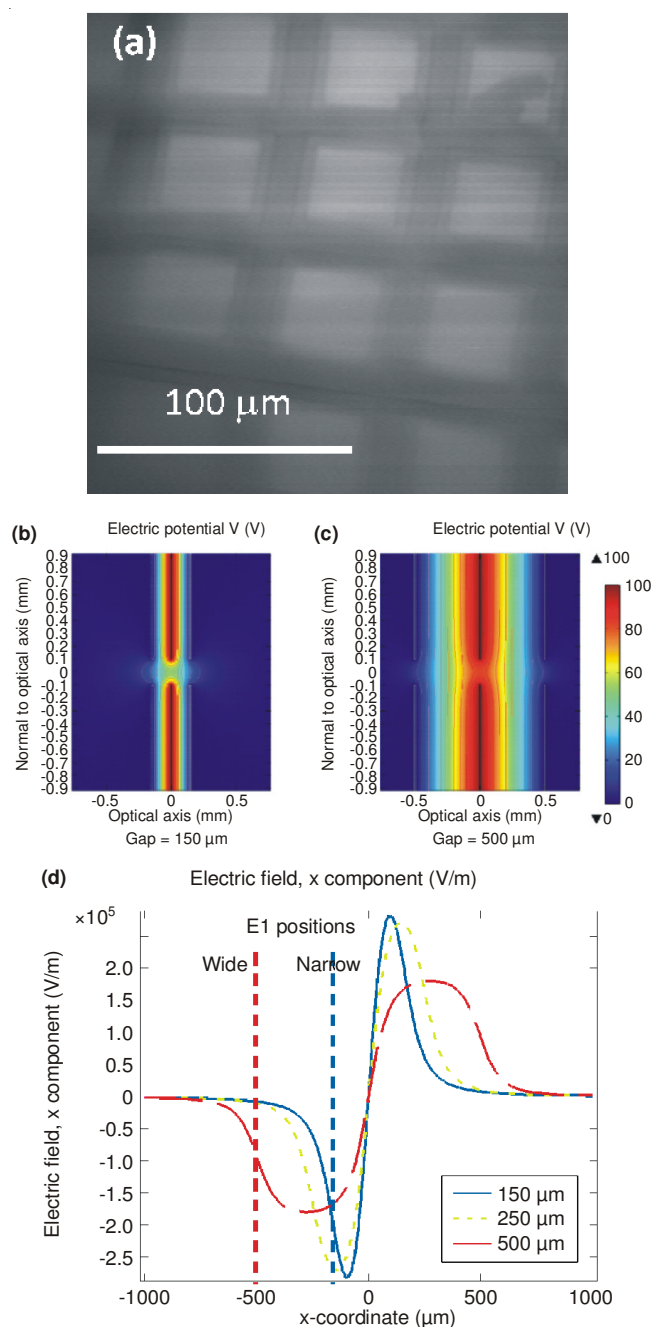


Fig. 6. (a) Electron micrograph of a grid sample from type-N microcolumn in Einzel lens (E2) focusing mode. (b) and (c) are surface plots of electric potential for the Einzel lenses with the electrode gap of 150 and 500  $\mu\text{m}$ , respectively. The plots are obtained from 2D Einzel lens modeling in which 100 V is applied on the central electrode (E2) and other electrodes are grounded. (d) Line plot of x-component of electric field along the optical axis (x-coordinate) for gap between electrodes 150, 250 and 500  $\mu\text{m}$ . Red and blue vertical broken lines show the position of E1 for type-W and type-N microcolumn, respectively

(E1 and E3) were grounded. These surface plots show that electric potential is symmetrically distributed and is gradually decreasing toward E1 or E3 electrode from the highest potential at E2 electrode.

Conspicuously, the electric potential is prolonged out beyond E1 and E3 electrodes through their apertures when the gap is narrow (Fig. 6(b)) while it is restrained inside the Einzel lens region when the gap is wide (Fig. 6(c)).

The variations of electric field strength along the optical axis are plotted in Fig. 6(d) for the Einzel lenses with the electrode gap of 150, 250 and 500  $\mu\text{m}$ . These plots display symmetrical distribution of electric field strength with respect to the center electrode. There are two extreme points which lie either between E1 and E2 or E2 and E3. The important point is that the extreme value is larger when the gap is smaller. That is, the maximum electric field strength is 0.285 MV/m for  $d = 150 \mu\text{m}$ , while that for  $d = 500 \mu\text{m}$  is 0.180 MV/m. This fact indicates that we can get stronger electric field by narrowing the electrode gap at the same focusing voltage. On the other hand, the narrow gap structure generates so strong electric field beyond E1 or E3 apertures (Fig. 6(d)) that it possibly interferes with the electric field produced by nearby structures such as deflectors or target. This interference produces some electrical noise which will make the focus unclear and result in blurry-distorted images. Hence, we shifted to the two-lens focusing mode for better image quality and larger scan range.

Two-lens focusing mode (both S2 and E2 electrodes are biased simultaneously) was performed with type-N microcolumn and the electron micrographs acquired in this mode are presented in Fig. 7. The images of Fig. 7(a-d) were acquired at E2 voltages of 150, 200, 250 and 290 V, respectively with S2 voltage fixed at -265 V and tip voltage at -300 V. In the micrographs, the Cu grid meshes appeared distinct and relatively better resolved compared with the images obtained in one lens E2 focusing mode. The images become clear with increasing E2 voltage though some edge distortion is accompanied. The interference of electric field produced by Einzel lens and deflector probably makes distorted image at the corner side.

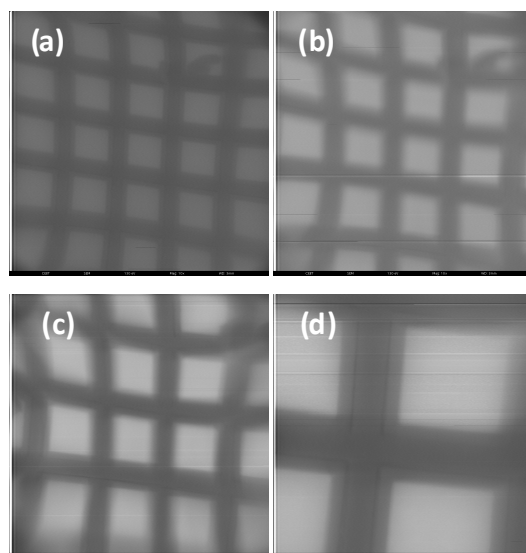


Fig. 7. Electron micrographs of a grid sample obtained with type-N microcolumn in two-lens focusing mode at E2 voltages of 150 V (a), 200 V (b), 250 V (c) and 290 V (d). Images (a)-(c) were acquired with the deflector voltage of  $\pm 45 \text{ V}$  and image (d) was with  $\pm 20 \text{ V}$

To understand the effect of gap between electrodes of Einzel lens in two-lens focusing mode, simulation analysis on e-beam trajectories were performed using commercially available tool, OPERA. Fig. 8 displays the simulation results

on one-lens (Fig. 8a) and two-lens focusing mode (Fig. 8b) for gap of 150 and 500  $\mu\text{m}$ . In Fig. 8a, simulation was performed by applying a bias voltage of -240 V to S2 electrode only and in Fig. 8b, it was performed by applying a bias voltage of 500 V to E2 electrode while S2 voltage was kept constant ( $V_{S2} = -240 \text{ V}$ ).

In order to obtain the field of view in each configuration, we increased the deflector voltage until the e-beam is cut by the edge of Einzel lens aperture and the beams presented in Fig. 8a and 8b are simulated results just before the aperture edge start to cut the e-beam. The deflector voltages meeting this condition were:  $\pm 38, \pm 35$  and  $\pm 28 \text{ V}$  in one-lens focusing mode and  $\pm 50, \pm 45$  and  $\pm 38 \text{ V}$  in two-lens focusing mode for gap between electrodes of 150, 250 and 500  $\mu\text{m}$ , respectively. In Fig. 8 the positions of three corresponding electrodes of source and Einzel lens are shown by broken black lines and broken-dot blue lines, respectively. Noticeably, a sharp bending of e-beam is observed at Einzel lens region in two lens focusing mode.

To find the scan ranges, we measured the e-beam deflections from the optical axis (blue double arrow lines in Fig. 8a and b) to the center of beam at focal planes. The scan ranges are plotted in Fig. 8c with solid squares in one-lens (S2) focusing mode. In this mode, the scan range decreases with increasing gap which is consistent with experimental data (Fig. 4c). On the contrary, in two-lens focusing mode, the scan range increases with increasing gap as depicted by the open circles.

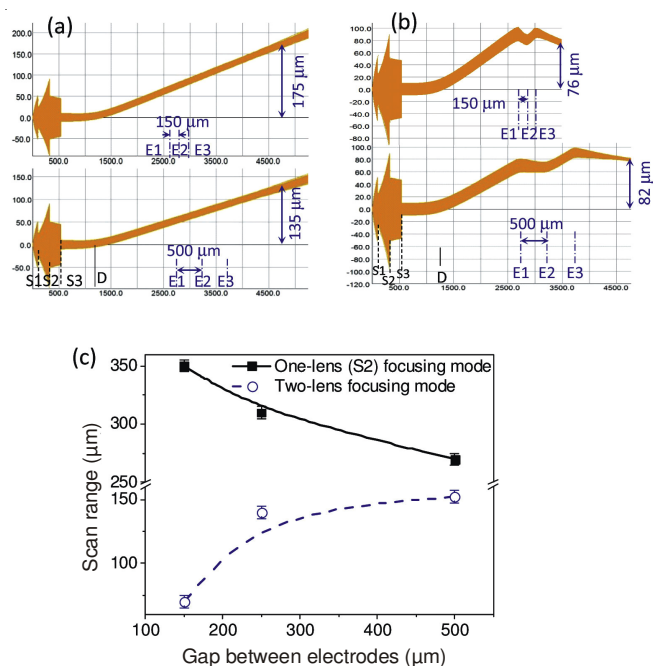


Fig. 8. Electrodynamic simulation of e-beam trajectories for type-N and type-W microcolumns. Beam trajectories in (a) one-lens focusing mode, (b) two-lens focusing mode, (c) scan range variation with the variation of gap between electrodes for both one-lens and two-lens focusing mode

These simulation and experimental results illustrate that scan range varies with gap between electrodes of Einzel lens and the operation mode. It is larger for type-N microcolumn than type-W microcolumn in source lens focusing mode but opposite in two-lens focusing mode. This phenomenon can

be illustrated as follows. In source lens (S2) focusing mode operation, the total e-beam travelling path in Einzel lens region is shorter for narrow gap (type-N) than wider gap (type-W) while the aperture diameter is same. This will provide larger solid angle to e-beam at the exit aperture and the beam can scan larger area in type-N than type-W. This effect dominates in source-lens focusing mode only since the beam path is not straight when E2 electrode is biased. However, in the two-lens focusing mode, the scan range is reduced in type-N microcolumn because the electric field from Einzel lens strongly confines the e-beam along the axial line. For the type-W microcolumn, the scan range is larger in two-lens focusing mode because the relatively weaker electric field does not confine the e-beam along the axis only. It also allows to swing the beam far from axis. Hence, according to necessity, we can adjust the gap between lens-electrode and the mode of operations.

### Conclusion

Electrostatic lenses with flexible gap between electrodes were fabricated from thin Si membrane using MEMS technology for e-beam microcolumn and its performances were evaluated with imaging technique. Further analytical study on scan ranges and image quality was carried out with the help of computer simulation. First a thin Si membrane was fabricated with an aperture whose size and shape was well defined with geometrical perfectness following photo-lithography, deep RIE and wet etching. The fabricated membrane was bonded with pre-fabricated Pyrex chip for insulating gap between electrodes and supporting substrate. Multiple electrodes were aligned through their apertures by laser diffraction alignment technique and bonded for completing source/Einzel lens. Two types of microcolumns, type-N and type-W were assembled using two different Einzel lens structures with gaps between electrodes of 150 and 500  $\mu\text{m}$ .

The microcolumn were separately operated in two modes of operation: one-lens and two-lens focusing mode. For analytical study, an electrostatics simulation was performed using

a commercial finite element analysis software. It was observed that the scan range increases with narrowing gap between electrodes and tip voltage in source lens focusing mode. But the results were opposite for two-lens focusing mode.

Therefore, the gap between Einzel lens is required to be adjusted for scan range and image quality according to the mode of operations.

### ACKNOWLEDGEMENTS

This work is supported from the IT R & D program of Ministry of Knowledge Economy (MKE)/Korea Evaluation Institute of Industrial Technology (KEIT) (No. 10039226), "Development of Actinic EUV Mask Inspection Tool and Multiple Electron Beam Wafer Inspection Technology."

### REFERENCES

1. S.Y. Chen, H.T. Ng, S.Y. Ma, H.H. Chen, C.H. Liu and K.Y. Tsai, *J. Vac. Sci. Technol. B*, **29**, 06FD04 (2011).
2. L.P. Muray, *Scanning*, **33**, 155 (2011).
3. Y.C. Kim, D.W. Kim, S. Ahn, T.S. Oh, J.B. Kim, Y.S. Roh, D.G. Hasko and H.S. Kim, *J. Vac. Sci. Technol. B*, **27**, 3208 (2009).
4. T.S. Oh, D.W. Kim, Y.C. Kim, S. Ahn, G.H. Lee and H.S. Kim, *J. Vac. Sci. Technol. B*, **28**, C6C69 (2010).
5. E. Kratschmer, H.S. Kim, M.G.R. Thomson, K.Y. Lee, S.A. Rishton, M.L. Yu and T.H.P. Chang, *J. Vac. Sci. Technol. B*, **13**, 2498 (1995).
6. J.P. Spallas, C.S. Silver, L.P. Muray, T. Wells and M. El-Gomati, *Microelectron Eng.*, **83**, 984 (2006).
7. L.P. Muray, C.S. Silver and J.P. Spallas, *J. Vac. Sci. Technol. B*, **24**, 2945 (2006).
8. R. Saini, Z. Jandric, I. Gory, S.A.M. Mentink and D. Tuggle, *J. Vac. Sci. Technol. B*, **24**, 813 (2006).
9. M.G.R. Thomson and T.H.P. Chang, *J. Vac. Sci. Technol. B*, **13**, 2445 (1995).
10. J.P. Spallas, C.S. Silver and L.P. Muray, *J. Vac. Sci. Technol. B*, **24**, 2892 (2006).
11. T.H.P. Chang, D.P. Kern and L.P. Muray, *J. Vac. Sci. Technol. B*, **8**, 1698 (1990).
12. T.H.P. Chang, M.G.R. Thomson, M.L. Yu, E. Kratschmer, H.S. Kim, K.Y. Lee, S.A. Rishton and S. Zolgharnain, *Microelectron Eng.*, **32**, 113 (1996).